

# Neutron Scattering and Spectroscopic Studies of Hydrogen Adsorption in $\text{Cr}_3(\text{BTC})_2$ —A Metal–Organic Framework with Exposed $\text{Cr}^{2+}$ Sites

Kenji Sumida,<sup>†</sup> Jae-Hyuk Her,<sup>‡,§,⊥</sup> Mircea Dinca,<sup>†,‡,¶</sup> Leslie J. Murray,<sup>†,○</sup> Jennifer M. Schloss,<sup>||</sup> Christopher J. Pierce,<sup>||</sup> Benjamin A. Thompson,<sup>||</sup> Stephen A. FitzGerald,<sup>\*,||</sup> Craig M. Brown,<sup>\*,§</sup> and Jeffrey R. Long<sup>\*,†</sup>

<sup>†</sup>Department of Chemistry, University of California, Berkeley, California 94720, and Materials Sciences Division, Lawrence Berkeley National Laboratory, Berkeley, California 94720

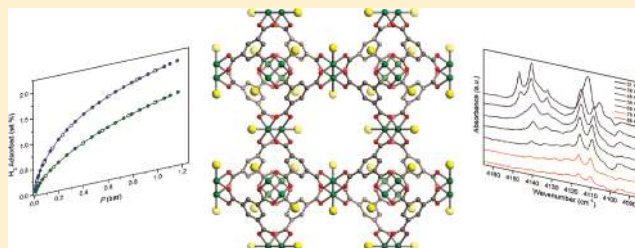
<sup>‡</sup>Department of Materials Science and Engineering, University of Maryland, College Park, Maryland 20742

<sup>§</sup>National Institute of Standards and Technology, Center for Neutron Research, Gaithersburg, Maryland 20899

<sup>||</sup>Department of Physics, Oberlin College, Oberlin, Ohio 44074

## Supporting Information

**ABSTRACT:** Microporous metal–organic frameworks possessing exposed metal cation sites on the pore surface are of particular interest for high-density  $\text{H}_2$  storage at ambient temperatures, owing to the potential for  $\text{H}_2$  binding at the appropriate isosteric heat of adsorption for reversible storage at room temperature (ca.  $-20$  kJ/mol). The structure of  $\text{Cr}_3(\text{BTC})_2$  ( $\text{BTC}^{3-} = 1,3,5\text{-benzenetricarboxylate}$ ) consists of dinuclear paddlewheel secondary building units connected by triangular  $\text{BTC}^{3-}$  bridging ligands to form a three-dimensional, cubic framework. The fully desolvated form of the compound exhibits BET and Langmuir surface areas of 1810 and 2040  $\text{m}^2/\text{g}$ , respectively, with open axial  $\text{Cr}^{2+}$  coordination sites on the paddlewheel units. Its relatively high surface area facilitates  $\text{H}_2$  uptakes (1 bar) of 1.9 wt % at 77 K and 1.3 wt % at 87 K, and a virial-type fitting to the data yields a zero-coverage isosteric heat of adsorption of  $-7.4(1)$  kJ/mol. The detailed hydrogen loading characteristics of  $\text{Cr}_3(\text{BTC})_2$  have been probed using both neutron powder diffraction and inelastic neutron scattering experiments, revealing that the  $\text{Cr}^{2+}$  site is only partially populated until a marked elongation of the Cr–Cr internuclear distance occurs at a loading of greater than 1.0  $\text{D}_2$  per  $\text{Cr}^{2+}$  site. Below this loading, the  $\text{D}_2$  is adsorbed primarily at the apertures of the octahedral cages. The H–H stretching frequency corresponding to  $\text{H}_2$  molecules bound to the primary site is observed in the form of an *ortho*–*para* pair at 4110 and 4116  $\text{cm}^{-1}$ , respectively, which is significantly shifted compared to the frequencies for free  $\text{H}_2$  of 4155 and 4161  $\text{cm}^{-1}$ . The infrared data have been used to compute a site-specific binding enthalpy for  $\text{H}_2$  of  $-6.7(5)$  kJ/mol, which is in agreement with the zero-coverage isosteric heat of adsorption derived from gas sorption isotherm data.



## INTRODUCTION

Metal–organic frameworks have attracted significant interest in recent years, in part owing to their potential applications in gas storage, molecular separations, and heterogeneous catalysis.<sup>1</sup> In particular, the ability to construct these materials from the combination of a judiciously selected metal ion and organic bridging unit may provide a versatile platform for the preparation of materials possessing physical and chemical properties that are finely tuned for specific applications. With regard to hydrogen storage for mobile applications, gravimetric and volumetric storage densities approaching those prescribed by the U.S. Department of Energy<sup>2</sup> have been observed within the highest surface-area metal–organic frameworks at cryogenic temperatures.<sup>3</sup> However, the storage capacity within these materials greatly diminishes at ambient temperature owing to the weak physisorptive interactions that predominate between  $\text{H}_2$  and the framework surface. Indeed, the zero-coverage isosteric heat

of adsorption within these materials typically lies in the range of  $-5$  to  $-7$  kJ/mol, which is far below the  $-15$  kJ/mol considered optimal over the entire adsorption range for an adsorbent operating between 1.5 and 30 bar at 298 K.<sup>4</sup> Furthermore, the inclusion of an enthalpy–entropy correlation increases this magnitude even further, suggesting an optimal enthalpy of adsorption in the range of  $-20$  to  $-25$  kJ/mol.<sup>5</sup>

One strategy for improving the isosteric heat of  $\text{H}_2$  adsorption within metal–organic frameworks is the synthesis of materials possessing open metal cation sites on the pore surface.<sup>6</sup> Here, the charge of the cation serves to induce a dipole on the  $\text{H}_2$  molecule, resulting in an electrostatic interaction that is stronger than the

Received: January 21, 2011

Revised: March 7, 2011

Published: March 25, 2011

dispersion-type interactions that predominate for physisorbed molecules.<sup>6,7</sup> Indeed, a zero-coverage isosteric heat of H<sub>2</sub> adsorption as high as −15.1 kJ/mol has been demonstrated within the material Co<sub>4</sub>(H<sub>2</sub>O)<sub>4</sub>(MTB)<sub>2</sub> (H<sub>4</sub>MTB = methanetetra benzoic acid), which features unsaturated Co<sup>2+</sup> sites following activation.<sup>8</sup> However, in this case, the isosteric heat rapidly decreases as a function of surface coverage, indicating that the density of strong binding sites is a crucial factor in facilitating large H<sub>2</sub> storage capacities at 298 K.<sup>9</sup> Thus, increasing the density of open metal sites remains a significant synthetic challenge, and a substantial body of recent computational work has been devoted to identifying potential candidate materials.<sup>10</sup>

The microporous metal–organic framework Cr<sub>3</sub>(BTC)<sub>2</sub> (Figure 1, H<sub>3</sub>BTC = 1,3,5-benzenetricarboxylic acid)<sup>11</sup> features a cubic network (space group: *Fm-3m*) of dinuclear paddlewheel units linked by triangular BTC<sup>3−</sup> organic bridging units to form a (3,4)-net that is isostructural with M<sub>3</sub>(BTC)<sub>2</sub> (M = Cu, Mo).<sup>12,13</sup> Here, six paddlewheel units and four BTC<sup>3−</sup> ligands form octahedral cages that share vertices to form a three-dimensional pore system resembling the boracite net topology. Upon desolvation of the solid by heating *in vacuo*, the material possesses unsaturated Cr<sup>2+</sup> sites at the paddlewheel units. The presence of these sites has recently been demonstrated to afford tremendous adsorption selectivity for O<sub>2</sub> over N<sub>2</sub>, owing to the ability of the metal centers to engage in a partial electron transfer with O<sub>2</sub>, but not N<sub>2</sub>.<sup>11</sup> Although such an interaction was not expected to occur with H<sub>2</sub>, the high charge density at these coordination sites could still be of benefit for H<sub>2</sub> adsorption. Herein, we report the H<sub>2</sub> storage properties of Cr<sub>3</sub>(BTC)<sub>2</sub>, as probed through low-pressure adsorption experiments, infrared spectroscopy, and neutron scattering studies. The complementary nature of the experiments offers a greater depth in the description of H<sub>2</sub> adsorption within the material, and results in a more complete understanding of the influence of various chemical and structural features on the adsorption properties.

## EXPERIMENTAL SECTION

**General Considerations.**<sup>14</sup> Cr<sub>3</sub>(BTC)<sub>2</sub> was synthesized and activated according to the literature procedure.<sup>11</sup> All reagents were obtained from commercial vendors, and used without further purification. All powder X-ray diffraction patterns were collected using a Bruker D8 Advance diffractometer (Cu K<sub>α</sub>; λ = 1.5406 Å) equipped with a capillary stage. Owing to the air and moisture sensitivity of Cr<sub>3</sub>(BTC)<sub>2</sub>, all manipulations were performed within a glovebox under a dinitrogen or argon atmosphere. Note that even brief exposure of the compound to the air induces an immediate color change of the solid to a dark forest green color, which is accompanied by a loss of crystallinity and porosity. The isosteric heat of H<sub>2</sub> adsorption was calculated using the method reported previously.<sup>6f</sup>

**Low-Pressure Gas Sorption Measurements.** Glass sample tubes of a known weight were loaded with approximately 100 mg of sample, and sealed using a TranSeal. Samples were degassed at 160 °C for 24 h on a Micromeritics ASAP 2020 analyzer until the outgas rate was no more than 1 mTorr/min. The degassed sample and sample tube were weighed precisely and then transferred back to the analyzer. The outgas rate was again confirmed to be less than 1 mTorr/min. H<sub>2</sub> adsorption isotherms were measured at 77 K in a liquid nitrogen bath and at 87 K in a liquid argon bath.

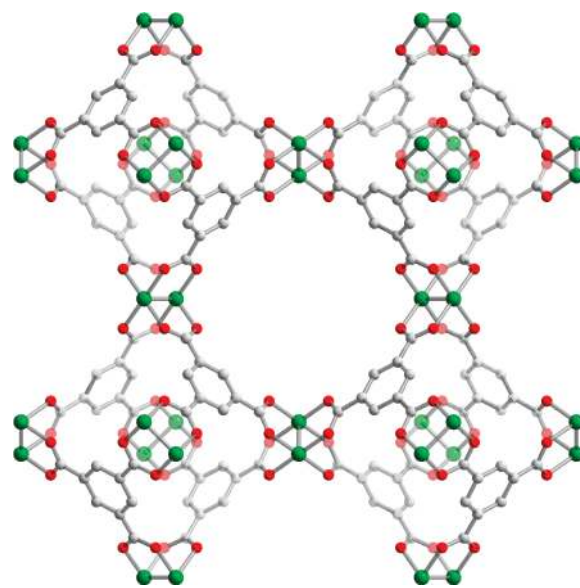


**Figure 1.** A portion of the crystal structure of evacuated Cr<sub>3</sub>(BTC)<sub>2</sub>. Green, gray, and red spheres represent Cr, C, and O atoms, respectively. Hydrogen atoms have been omitted for clarity.

**Neutron Powder Diffraction Measurements.** Neutron powder diffraction data were collected on the high resolution neutron powder diffractometer BT-1 at the National Institute of Standards and Technology (NIST) Center for Neutron Research (NCNR) with a Ge-(311) monochromator and using in-pile collimation of 15 min of arc, corresponding to a wavelength of 2.0782 Å. Measurements were taken as a function of deuterium loading (0.5, 1.0, 1.5, 2.0, and 3.0 D<sub>2</sub> molecules per Cr<sup>2+</sup> site, loading performed at ca. 60 K) at a temperature of ca. 4 K with a measurement time of ca. 9 h. Note that D<sub>2</sub> is used rather than H<sub>2</sub> owing to the large incoherent scattering cross section of H<sub>2</sub>, which results in an increased background and poorer quality diffraction data. The minor differences in properties between H<sub>2</sub> and D<sub>2</sub>, most notably their zero-point energies, are not expected to significantly affect the adsorption behavior within the framework in the context of the diffraction studies.

All sample transfers were performed in a helium-filled glovebox equipped with water and oxygen monitors. Initial sample activation was performed in a glass tube with a packless bellows valve attached. The sample was evacuated using a turbomolecular pump (10<sup>−5</sup> Torr) and heated to 150 °C for 48 h, after which time the sample was cooled and transferred to a cylindrical vanadium can equipped with a capillary gas line and a packless valve, and sealed with an indium O-ring. The sample was mounted onto a sample stick equipped with a stainless-steel gas line with an additional valve for a top-loading closed-cycle helium refrigerator. The sample was further degassed *in situ* under high vacuum to remove residual helium. During the experiments, a known amount of hydrogen (deuterium) gas was loaded into the sample (1.174 g), which was typically maintained at a temperature of 60 K (CCR) until no pressure drop was observed for at least 1 min. The sample was then cooled down to the base temperature of 3.5 K over a period of 1 h in order to perform measurements. In all cases, the outgas pressure reading was zero well before reaching 25 K.

Neutron powder diffraction patterns were analyzed using the Rietveld refinement method. The program EXPGUI<sup>15</sup> incorporating

the Rietveld program GSAS<sup>16</sup> was used to perform all refinements. The model of the bare material was refined first, and was used as the starting point for subsequent refinements of the D<sub>2</sub>-loaded samples. In all cases, D<sub>2</sub> molecules were treated as point scatterers with double occupancy in accord with the rotationally disordered quantum mechanical molecule.<sup>17</sup> The coordinates of all other atoms and the displacement parameters were allowed to vary during the refinement of each D<sub>2</sub> loading case. On the basis of the structure obtained from the diffraction pattern of the bare material, the diffraction patterns of the first D<sub>2</sub>-loaded case (0.5 D<sub>2</sub> molecules per Cr<sup>2+</sup>) were analyzed by first neglecting the D<sub>2</sub> molecules. The Fourier difference maps were calculated, clearly indicating the positions of D<sub>2</sub> adsorption sites. Accurate values for the D<sub>2</sub> locations and occupancy numbers were then obtained by Rietveld refinement after incorporating the D<sub>2</sub> molecules into the structure model. For each successive D<sub>2</sub> loading, the Fourier difference map was calculated on the basis of the results of the previous D<sub>2</sub> loading and used to identify new D<sub>2</sub> adsorption sites.

**Inelastic Neutron Scattering (INS) Spectroscopy.** The INS spectra were measured at 4 K using the pyrolytic graphite monochromator and 20'–20' collimation options on the BT-4 filter analyzer neutron spectrometer (FANS)<sup>18</sup> at the NCNR. The sample (1.174 g) was sealed in a cylindrical aluminum cell suitable for *in situ* gas loading and cooled in a CCR. H<sub>2</sub> gas was used during the measurements to take advantage of its large incoherent neutron scattering cross section. Note that the H<sub>2</sub> molecule is a very good quantum rotor due to its light mass and consists of two indistinguishable fermions (protons) that require the wave function to be antisymmetric. If the nuclear spins of two protons are antiparallel, H<sub>2</sub> is said to be in a *para* state (*p*-H<sub>2</sub>); otherwise, it is in an *ortho* state (*o*-H<sub>2</sub>). The quantum rotation number, *J*, of a H<sub>2</sub> molecule thus has to be even for a *para*-H<sub>2</sub> and odd for an *ortho*-H<sub>2</sub>. At room temperature, only one-fourth of H<sub>2</sub> molecules are in the *para* state. Usually, the conversion rate between states is very slow but can be greatly accelerated in the presence of a fluctuating magnetic moment. Both *p*-H<sub>2</sub> and normal H<sub>2</sub> (*n*-H<sub>2</sub>), which consists of 25% *p*-H<sub>2</sub> and 75% *o*-H<sub>2</sub>, were used in these experiments.

A neutron scattered by a H<sub>2</sub> molecule can induce the required nuclear spin flip to convert a *para/ortho* H<sub>2</sub> to an *ortho/para* H<sub>2</sub>. This *para*–*ortho* or *ortho*–*para* transition is associated with the change of the rotational quantum number, *J*, from even/odd to odd/even, and has a large neutron scattering cross section that is proportional to the incoherent neutron scattering cross section of the proton. INS spectra of the adsorbed H<sub>2</sub> were obtained by subtracting the INS spectrum of the bare materials. For a free hydrogen molecule, the *para*–*ortho* transition is usually associated with the *J* = 0 to *J* = 1 excitation occurring with an energy of 14.7 meV, which can be directly measured by INS but not optical spectroscopies. The local potential of a host material will generate rotational barriers for the adsorbed H<sub>2</sub> which typically cause the *J* = 1 state to split into its three sublevels. Additionally, the translation excitations of the H<sub>2</sub> molecule may be coupled to the rotational transition and complicate the observed spectra. Hence, the INS spectra of adsorbed H<sub>2</sub> may show complex features with multiple peaks in the spectrum containing rich information about the host material and the hydrogen interactions.

Loadings of 0.5, 1.0, 2.0, and 3.0 *p*-H<sub>2</sub> and *n*-H<sub>2</sub> per Cr<sup>2+</sup> site were performed at 70 K with data collection at 4 K. Data were collected for approximately 9 h per loading. The energy resolution is between 1.2 and 2.0 meV over the energy transfer ranges accessible. Data reduction, including the subtraction of the bare

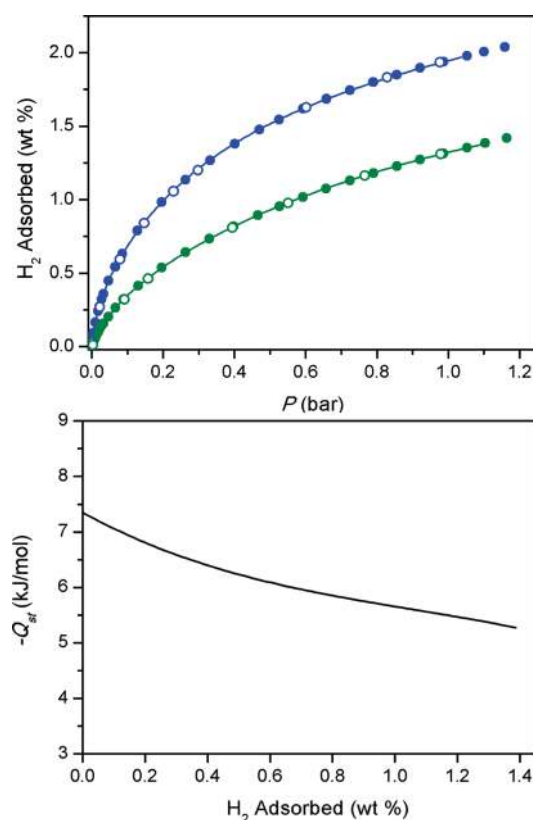


**Figure 2.** (upper) Lower-pressure H<sub>2</sub> isotherms in Cr<sub>3</sub>(BTC)<sub>2</sub> collected at 77 K (blue) and 87 K (green). Closed and open symbols represent adsorption and desorption, respectively, and the solid lines represent a virial-type fitting to the data. (lower) A plot of the isosteric heat of adsorption as a function of the conversion of H<sub>2</sub> coverage.

Cr<sub>3</sub>(BTC)<sub>2</sub> spectrum from the H<sub>2</sub>-loaded spectra, and peak fitting, were performed within the DAVE software suite.<sup>19</sup>

**Infrared Spectroscopy.** Infrared spectra were acquired using a Bomem DA3 Michelson interferometer equipped with a quartz-halogen source, a CaF<sub>2</sub> beamsplitter, and a liquid nitrogen cooled mercury-cadmium-telluride detector. A custom-built diffuse reflectance system<sup>20</sup> with a sample chamber that allows both the temperature and atmosphere of the material to be controlled was utilized for all experiments. Powder samples of Cr<sub>3</sub>(BTC)<sub>2</sub> (ca. 10 mg) were transferred under an inert atmosphere to a cup affixed to a copper slab providing thermal contact to a coldfinger cryostat (Janis ST-300T). The sample temperature was monitored by a Si-diode thermometer placed directly within the sample cup. Prior to introduction of the hydrogen gas, the samples were evacuated for several hours at room temperature. Known quantities of research grade (99.9999% purity) H<sub>2</sub> were dispensed from a calibrated gas manifold by monitoring the change in pressure.

## RESULTS AND DISCUSSION

**H<sub>2</sub> Adsorption Isotherms.** The H<sub>2</sub> adsorption isotherms collected for an activated sample of Cr<sub>3</sub>(BTC)<sub>2</sub> are presented in Figure 2. The relatively high BET surface area of 1810 m<sup>2</sup>/g facilitates a reversible adsorption (1 bar) of 1.9 and 1.3 wt % at 77 and 87 K, respectively. The zero-coverage isosteric heat of adsorption (Q<sub>st</sub>) for H<sub>2</sub> obtained from a virial-type fitting to the isotherm data of -7.4(2) kJ/mol represents just a slight increase in



the magnitude of  $Q_{st}$  compared to materials that do not feature exposed cation sites. As discussed below, the neutron powder diffraction data reveal that the  $Cr^{2+}$  sites are occupied only at high loadings following a slight elongation of the Cr–Cr distance within the paddlewheel unit. As a result, this leads to the occupation of a single binding site that facilitates short contacts with the organic component of the framework at low coverage, which is consistent with the relatively small magnitude of  $Q_{st}$ . Note that this serves to highlight one of the primary disadvantages of the analysis of bulk isotherm data, as is often performed in adsorption studies, since conclusions regarding the binding environment of  $H_2$  within the framework cannot be deduced directly, particularly in cases where the site-specific adsorption enthalpies of two or more sites within the unit cell are quite similar. Nevertheless, the value of  $Q_{st}$  at zero coverage is comparable to the corresponding value reported for  $Cu_3(BTC)_2$  ( $-6.8$  kJ/mol).<sup>21</sup> Consistent with the successive occupancy of the strongest binding sites within

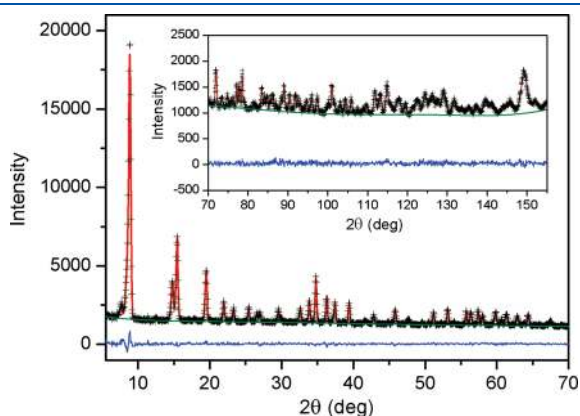


**Figure 3.** Representative neutron powder diffraction data, collected for  $Cr_3(BTC)_2$  following a dosing of 0.5  $D_2$  molecules per  $Cr^{2+}$  site. Green lines, crosses, and red lines represent the background, experimental, and calculated diffraction patterns, respectively. The blue line represents the difference between experimental and calculated patterns. The final Rietveld goodness-of-fit parameter was  $\chi^2 = 0.9329$ .

$Cr_3(BTC)_2$ , the magnitude of  $Q_{st}$  gradually decreases to  $-5.7(2)$  kJ/mol at a  $H_2$  uptake of 1.0 wt %. A complete analysis of the coverage-dependent adsorption characteristics and binding sites within the material is explored in detail below in the context of neutron powder diffraction, inelastic neutron scattering spectroscopy, and infrared spectroscopy.

**Neutron Powder Diffraction Data.** Rietveld analysis of the bare  $Cr_3(BTC)_2$  material revealed the expected cubic network of dinuclear paddlewheel secondary building units bridged by 3-connected organic linkers (Figure 1). Significantly, the short Cr–Cr distance of 2.06(2) Å is indicative of the presence of a metal–metal quadruple bond, and results in the  $Cr^{2+}$  being situated approximately 0.11(2) Å below the four-atom mean plane formed by the oxygen atoms of the carboxylate ligands. We note that, in the fully evacuated state, no nuclear density was observed on the axial coordination sites on the  $Cr^{2+}$  centers, reflecting the removal of all of the coordinated solvent molecules, and full activation of the pores.

The  $D_2$  binding sites within  $Cr_3(BTC)_2$  were determined by successively dosing the evacuated material with  $D_2$  at loadings corresponding to 0.5, 1.0, 1.5, 2.0, and 3.0  $D_2$  molecules per  $Cr^{2+}$  center, and taking nuclear density Fourier difference maps between the loaded and evacuated materials. Any new locations were added to the Rietveld process where the final positions and occupancies of the  $D_2$  molecules were allowed to refine freely. Note that, at each loading level, the total refined occupancy of  $D_2$  assigned from the neutron density map agrees well with the expected total occupancy, indicating full assignment of all of the binding sites within the unit cell (Tables S2–S6, Supporting Information).

The neutron diffraction data and Rietveld refinement results for data collected at a loading of 0.5  $D_2$  molecules per  $Cr^{2+}$  site are shown in Figure 3. Surprisingly, no nuclear density was observed at this loading level, and the  $D_2$  is located in the apertures of the octahedral cages at a distance of approximately 4 Å from the carbon atoms of the aryl rings of the  $BTC^{3-}$  ligands (Figure 4B, site I). Upon increasing the loading to 1.0  $D_2$  molecules per  $Cr^{2+}$  site, additional nuclear density was observed at site I, as well as a small quantity at the open  $Cr^{2+}$  site

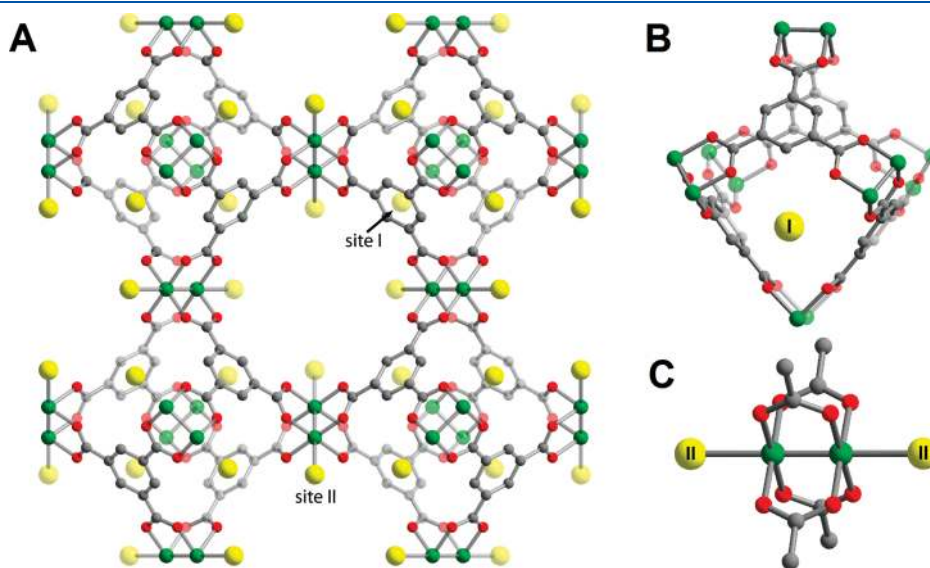


**Figure 4.** A portion of the structure of  $Cr_3(BTC)_2$  showing the first two  $D_2$  binding sites, where green, red, and gray spheres represent Cr, O, and C atoms, respectively, while large yellow spheres represent  $D_2$  molecules (A). The first occupied position (site I) is located at the apertures of the octahedral cages (B), while, at higher loadings, the unsaturated  $Cr^{2+}$  center (site II) is occupied (C).

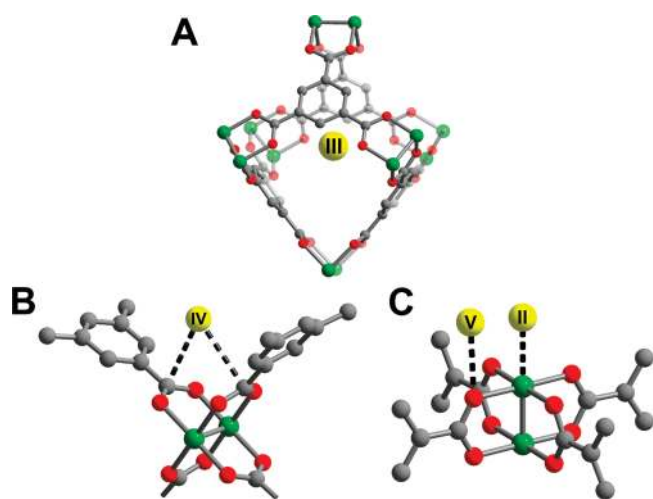


**Figure 5.** D<sub>2</sub> binding sites III–V observed within Cr<sub>3</sub>(BTC)<sub>2</sub> at higher loadings. Site III (A) lies in the center of the octahedral cages, site IV (B) resides within a V-shaped binding pocket between two BTC<sup>3−</sup> moieties, while site V (C) is situated in close contact (ca. 2.7 Å) with the oxygen atom of the carboxylate group.

(Figure 4C, site II). Here, the D<sub>2</sub> is disposed at a distance of 2.63(2) Å from the Cr<sup>2+</sup> center, which is significantly greater than the corresponding distance of 2.39(1) Å observed in Cu<sub>3</sub>(BTC)<sub>2</sub>,<sup>22</sup> and is also longer than those observed for other frameworks featuring exposed metal cation sites.<sup>23</sup> This is consistent with the larger ionic radius of Cr<sup>2+</sup> (0.80 Å; high spin) compared to Cu<sup>2+</sup> (0.73 Å), yielding a lower charge density and subsequently a weaker induced dipole on the adsorbed D<sub>2</sub> molecules.<sup>24</sup> Furthermore, the Cu–Cu distance in Cu<sub>3</sub>(BTC)<sub>2</sub> is significantly longer than the Cr–Cr distance in Cr<sub>3</sub>(BTC)<sub>2</sub>, which results in the Cu<sup>2+</sup> ions projecting out into the pores of the framework. This likely allows the D<sub>2</sub> molecules to interact more directly with the metal centers due to the lower steric demand of these sites. Here, the apparent preference for D<sub>2</sub> to populate site I rather than site II at the lowest loadings is probably a result of a combination of the Cr<sup>2+</sup> binding site being sterically less accessible to guest molecules and the binding energy at the open metal site being comparable to that of site I. Nevertheless, to our knowledge, Cr<sub>3</sub>(BTC)<sub>2</sub> is the first example of a metal–organic framework furnished with open metal sites wherein the metal center is not the favored binding site for D<sub>2</sub> at low coverages.

Interestingly, upon increasing the D<sub>2</sub> loading from 1.0 to 1.5 D<sub>2</sub> molecules per Cr<sup>2+</sup> center, an elongation of the Cr–Cr distance from 2.06(2) to 2.17(2) Å is observed, representing a decrease in the bond order of the Cr–Cr interaction. This serves to project the Cr<sup>2+</sup> cations above the four-atom mean plane of the oxygen atoms of the carboxylate moieties. Importantly, this structural change is accompanied by a reorganization of the nuclear density after the next dosing step such that site II is fully populated, suggesting that the D<sub>2</sub> molecules are able to more readily access the open metal site once it is projected out into the channels. Note that the sample is warmed to approximately 60 K during each dosing step, allowing the D<sub>2</sub> molecules to migrate more rapidly to their preferred positions following the structural change. Furthermore, at this loading level, additional nuclear density is also observed at the center of the octahedral cages (Figure 5A, site III), and is observed at full occupancy. As the

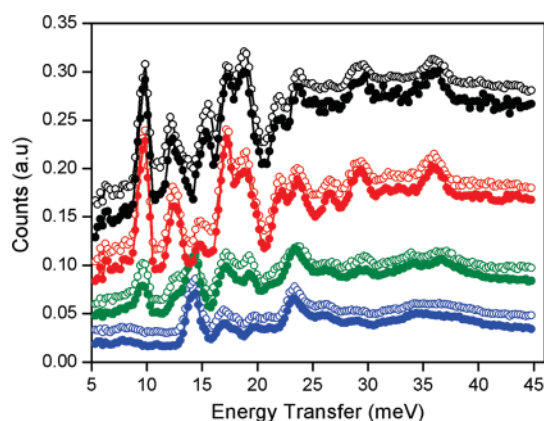


**Figure 6.** Selected inelastic neutron scattering (INS) spectra recorded at 4 K following subtraction of the spectrum of evacuated Cr<sub>3</sub>(BTC)<sub>2</sub> for loadings of 0.5 (blue), 1.0 (green), 2.0 (red), and 3.0 (black) H<sub>2</sub> molecules per Cr<sup>2+</sup> site. Filled and open symbols represent data for *p*-H<sub>2</sub> and *n*-H<sub>2</sub>, respectively.

loading is increased further to 2.0 and 3.0 D<sub>2</sub> molecules per Cr<sup>2+</sup> site, additional nuclear density appears, corresponding to close contacts in the channels of the framework. As shown in Figure 5B, site IV is positioned in a V-shaped binding pocket formed by two carboxylate moieties of the paddlewheel units, wherein the D<sub>2</sub> molecule is disposed approximately 3.3 Å from the framework surface. Meanwhile, site V (Figure 5C) is observed approximately 2.8 Å from the oxygen atoms of the carboxylate moieties, although only a small occupancy is observed at this site even at the highest loadings. Previous studies performed on Cu<sub>3</sub>(BTC)<sub>2</sub> revealed adsorption sites with coordinates and interaction distances similar to sites III–V observed here,<sup>22</sup> which might be anticipated on the basis of the isostructural nature of the two frameworks.

**Inelastic Neutron Scattering Spectra.** The H<sub>2</sub> loading characteristics of Cr<sub>3</sub>(BTC)<sub>2</sub> were examined in further detail by inelastic neutron scattering. Data were collected at the same loadings (0.5, 1.0, 2.0, and 3.0 H<sub>2</sub> molecules per Cr<sup>2+</sup> site) as for the neutron powder diffraction experiments to allow for the best opportunity for correlation of FANS spectra with the binding sites observed crystallographically. For all spectra, routine data reduction and subtraction of the spectrum for the evacuated form of Cr<sub>3</sub>(BTC)<sub>2</sub> was performed, and selected spectra are displayed in Figure 6.

At the lowest loading of 0.5 H<sub>2</sub> per Cr<sup>2+</sup> site, a sharp peak is observed at 14.3 meV. This feature is consistent with the first transition between rotational energy levels,  $J = 0 \rightarrow 1$ , of an almost unhindered H<sub>2</sub> molecule, and presumably corresponds to the molecules located in the windows of the octahedral cages (site I). The lack of a significant shift for these molecules from the corresponding signal for free H<sub>2</sub> observed at 14.7 meV is presumably due to the relatively large distance between H<sub>2</sub> and the framework surface, resulting in only a small increase in the rotational barrier of the H<sub>2</sub> molecule upon occupation of site I. A broader feature is also observed at 23.0 meV, which is likely due to the rotation of H<sub>2</sub> coupled with a phonon of approximately 9 meV as observed in Cu<sub>3</sub>(BTC)<sub>2</sub>.<sup>17</sup> The overall similarity of the *n*-H<sub>2</sub> and *p*-H<sub>2</sub> spectra indicates that the normal hydrogen is converted from the  $J = 1$  *ortho* form to the  $J = 0$  *para* form, and this is mirrored for all loadings, even in the cases where the strongest accessible adsorption site is not the metal center. This

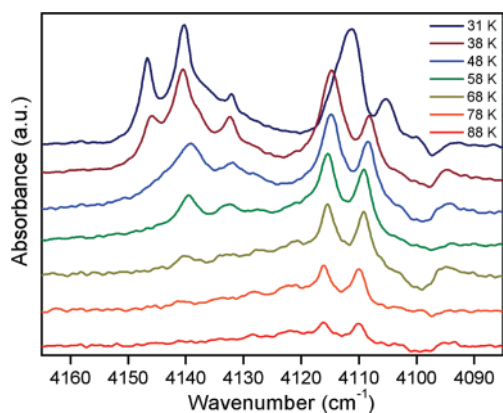


**Figure 7.** Selected variable-temperature infrared spectra (Q-region) for  $\text{Cr}_3(\text{BTC})_2$  following dosing with  $\text{H}_2$  collected at temperatures between 31 and 88 K at a resolution of  $1 \text{ cm}^{-1}$ . Spectra are offset for clarity.

suggests that virtually all of the  $\text{H}_2$  molecules are able to approach the paramagnetic  $\text{Cr}^{2+}$  ion with a sufficient proximity for *ortho*–*para* conversion.

Upon increasing the loading to 1.0  $\text{H}_2$  per  $\text{Cr}^{2+}$  site, a sharp feature at 9.6 meV is observed. This peak is assigned to  $\text{H}_2$  molecules bound to the unsaturated  $\text{Cr}^{2+}$  sites (site II), which experience a significant rotational hindrance due to the close approach of these molecules to the framework surface, as observed in the neutron powder diffraction experiments. Rotational transitions are also apparent at energies close to this value for *p*- $\text{H}_2$  in  $\text{Cu}_3(\text{BTC})_2$  where the initial adsorption is at the metal center.<sup>17</sup> The corresponding growth of a peak at around 19 meV is clearly observed and was previously ascribed to a coupled rotation and phonon in  $\text{Cu}_3(\text{BTC})_2$ , which is likely also the case here. The intensities of these peaks increase following subsequent loadings to 2.0 and 3.0  $\text{H}_2$  per  $\text{Cr}^{2+}$  site, which is consistent with the eventual full occupation of molecules at this binding site.

**Infrared Spectra.** The adsorption of  $\text{H}_2$  within  $\text{Cr}_3(\text{BTC})_2$  was further probed through the collection of variable-temperature infrared spectra. An activated sample of  $\text{Cr}_3(\text{BTC})_2$  was exposed to a total dosing of 4  $\text{H}_2$  per  $\text{Cr}^{2+}$  center. As the sample temperature was decreased, the  $\text{H}_2$  pressure dropped to a base value of 0.01 bar at 30 K, indicating that virtually all of the dosed gas had adsorbed onto the framework. The spectra collected at different temperatures during this procedure are presented in Figure 7. As the temperature is lowered from 88 K, the emergence of a single *ortho*–*para* pair corresponding to the H–H stretch for  $\text{H}_2$  molecules bound to the framework surface is observed at 4110 and 4116  $\text{cm}^{-1}$ , respectively. Here, the presence of only a single band at 88 K suggests the occupancy of a single crystallographic site within the unit cell, which, based on the neutron powder diffraction and INS experiments, is presumably the site located at the aperture of the octahedral cages (site I).<sup>25</sup>

Upon cooling of the sample below 58 K, a second *ortho*–*para* pair is observed at 4132 and 4141  $\text{cm}^{-1}$ , respectively. These bands are consistent with the occupation of a secondary binding site that is less polarizing toward  $\text{H}_2$  and, based upon the neutron diffraction data, is ascribed to adsorption of  $\text{H}_2$  at the open  $\text{Cr}^{2+}$  site (site II). Note that the reorganization of the neutron density following elongation of the Cr–Cr bond as observed in the neutron powder diffraction experiments suggests that the

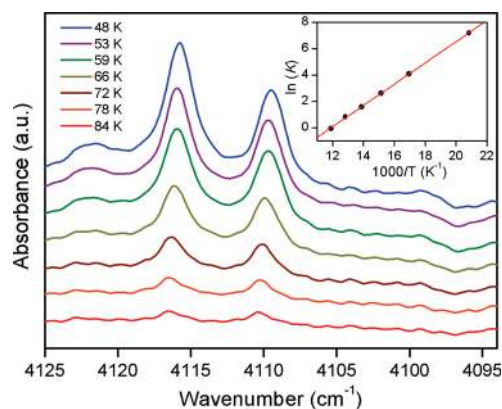


**Figure 8.** Selected variable-temperature infrared spectra of the *ortho*–*para* pair for  $\text{H}_2$  adsorbed at the primary binding site within  $\text{Cr}_3(\text{BTC})_2$  collected between 48 and 84 K at a resolution of  $1 \text{ cm}^{-1}$ . Spectra are offset for clarity. Inset: An Arrhenius law plot derived from the integrated absorbance from the spectral data.

interaction between  $\text{H}_2$  and  $\text{Cr}^{2+}$  is not necessarily weaker than the adsorption enthalpy for  $\text{H}_2$  at site I following the elongation of the Cr–Cr distance. This structural change, and the expected change in interaction energy, is expected to induce a shift in the position of the absorption band attributable to site II, owing to the change in the degree of activation of the  $\text{H}_2$  molecules located at this site. However, the relatively constant position of the adsorption bands for  $\text{H}_2$  at the  $\text{Cr}^{2+}$  site reveals that, under the conditions of the infrared experiments, such a structural change does not occur, possibly due to the significantly higher temperatures (and consequently small quantity of adsorbed  $\text{H}_2$ ) under which the data were collected.

The evolution of a single peak at 4146  $\text{cm}^{-1}$  is observed upon further cooling of the sample below 38 K. This new signal is attributed to adsorption of  $\text{H}_2$  at the center of the octahedral cages (site III), which was observed at high loadings in the neutron powder diffraction experiments. Notably, the occupation of this site induces a shift in the infrared absorption band for  $\text{H}_2$  located in the apertures of these cages (site I). This is presumably due to a change in the chemical environment for the  $\text{H}_2$  molecules at site I, owing to the relatively short proximity (ca. 3.4 Å) of site III from this site.

The lowest-temperature infrared data obtained for an  $\text{H}_2$  dosing of 1.1  $\text{H}_2$  per  $\text{Cr}^{2+}$  center are shown in Figure 8. The standard enthalpy of adsorption ( $\Delta H^0$ ) for the primary binding site was extracted by generating an Arrhenius-type plot from the integrated infrared absorbance as a function of temperature (see Figure 8, inset). The value of  $-6.7(5) \text{ kJ/mol}$  is consistent with the relatively weak binding of  $\text{H}_2$  at the primary binding site, and is significantly lower than the corresponding value obtained from a similar analysis for  $\text{Cu}_3(\text{BTC})_2$  ( $-10.1 \text{ kJ/mol}$ ).<sup>12c</sup> However, we note that the primary binding site in  $\text{Cu}_3(\text{BTC})_2$  is at the open  $\text{Cu}^{2+}$  cation sites, which leads to a higher site-specific adsorption enthalpy. In addition, the standard enthalpy change  $\Delta S^0$  of  $-78 \text{ J/mol}\cdot\text{K}$  is consistent with the close approach and efficient packing of the  $\text{H}_2$  molecules on the framework surface. Note that the enthalpy–entropy correlation for  $\text{H}_2$  adsorption is a significant factor in assessing the optimal value of  $\Delta H^0$  for metal–organic frameworks. The often-quoted optimal  $\Delta H^0$  value of ca.  $-15 \text{ kJ/mol}$  is based on a constant  $\Delta S^0 = 8R = -66.5 \text{ J/mol}\cdot\text{K}$ ,<sup>4</sup> which is smaller in magnitude than the value



observed here, and values obtained via similar variable-temperature infrared spectroscopy studies of  $\text{Cu}_3(\text{BTC})_2$ , and other porous media. The consideration of the higher magnitude of  $\Delta S^0$  leads to the optimal value for  $\Delta H^0$  being in the range of  $-20$  to  $-25$  kJ/mol.<sup>5</sup> Note that the value for  $\Delta S^0$  is binding-site-dependent, which suggests that the more a binding site imposes spatial ordering on the adsorbed  $\text{H}_2$  molecule, a larger magnitude of  $\Delta H^0$  is required to overcome the entropy contribution. Thus, the preparation of a metal–organic framework for ambient  $\text{H}_2$  storage applications requires careful consideration and fine-tuning of the thermodynamics of each binding site within the material.

**Conclusions.** The foregoing results demonstrate the hydrogen storage properties of  $\text{Cr}_3(\text{BTC})_2$ , a metal–organic framework possessing open  $\text{Cr}^{2+}$  sites, as probed through a combination of low-pressure adsorption, neutron powder diffraction, inelastic neutron scattering, and variable-temperature infrared experiments. Surprisingly, the loading characteristics differ significantly from those of the isostructural compound  $\text{Cu}_3(\text{BTC})_2$ , with full occupancy at the unsaturated  $\text{Cr}^{2+}$  center not being observed until a lengthening of the Cr–Cr distance also occurs at a loading of 1.5  $\text{D}_2$  per  $\text{Cr}^{2+}$  site. Although the low isosteric heat of adsorption in  $\text{Cr}_3(\text{BTC})_2$  precludes its application as a room temperature hydrogen storage material, such a detailed understanding of the hydrogen sorption properties as probed through several complementary experimental techniques has revealed greater insight into the chemical and physical properties required for next-generation hydrogen storage materials.

## ■ ASSOCIATED CONTENT

**Supporting Information.** Full experimental details, neutron powder diffraction refinement data, infrared spectra (PDF), and crystallographic information files (CIF). This material is available free of charge via the Internet at <http://pubs.acs.org>.

## ■ AUTHOR INFORMATION

### Present Addresses

<sup>†</sup>GE Global Research, Niskayuna, NY 12309.

<sup>#</sup>Department of Chemistry, Massachusetts Institute of Technology, Cambridge, Massachusetts, 02139.

<sup>○</sup>Department of Chemistry, University of Florida, Gainesville, Florida, 32611.

## ■ ACKNOWLEDGMENT

The research in Berkeley was funded by the Department of Energy under Contract No. DE-AC02-05CH11231. We acknowledge Fulbright New Zealand for partial support of K.S. The work at NIST was partially funded by the U.S. Department of Energy within the EERE Hydrogen Sorption Center of Excellence, and the work at Oberlin College was partially funded by the American Chemical Society Petroleum Research Fund. We thank Dr. Y. Liu for technical assistance during the neutron measurements.

## ■ REFERENCES

(1) (a) Eddaoudi, M.; Kim, J.; Rosi, N.; Vodak, D.; Wachter, J.; O’Keeffe, M.; Yaghi, O. M. *Science* **2002**, *295*, 469. (b) Matsuda, R.; Kitaura, R.;

Kitagawa, S.; Kubota, Y.; Belosludov, R. V.; Kobayashi, T. C.; Sakamoto, H.; Chiba, T.; Takata, M.; Kawazoe, Y.; Mita, Y. *Nature* **2005**, *436*, 238. (c) Millward, A. R.; Yaghi, O. M. *J. Am. Chem. Soc.* **2005**, *127*, 17998. (d) Furukawa, H.; Miller, M. A.; Yaghi, O. M. *J. Mater. Chem.* **2007**, *17*, 3197. (e) Ma, S.; Sun, D.; Simmons, J. M.; Collier, C. D.; Yuan, D.; Zhou, H. C. *J. Am. Chem. Soc.* **2008**, *130*, 1012. (f) Morris, R. E.; Wheatley, P. S. *Angew. Chem., Int. Ed.* **2008**, *47*, 4966. (g) Llewellyn, P. L.; Bourrelly, S.; Serre, C.; Vimont, A.; Daturi, M.; Hamon, L.; De Weireld, G.; Chang, J.-S.; Hong, D.-Y.; Hwang, Y. K.; Jhung, S. H.; Férey, G. *Langmuir* **2008**, *24*, 7245. (h) Furukawa, H.; Ko, N.; Go, Y. B.; Aratani, N.; Choi, S. B.; Choi, E.; Yazaydin, A. Ö.; Snurr, R. Q.; O’Keeffe, M.; Kim, J.; Yaghi, O. M. *Science* **2010**, *329*, 424.

(2) EERE: Hydrogen, Fuel Cells, & Infrastructure Technologies Program, <http://www.eere.energy.gov/hydrogenandfuelcells> (accessed August 2010).

(3) (a) Rosi, N. L.; Eckert, J.; Eddaoudi, M.; Vodak, D. T.; Kim, J.; O’Keeffe, M.; Yaghi, O. M. *Science* **2003**, *300*, 1127. (b) Férey, G.; Latroche, M.; Serre, C.; Millange, F.; Loiseau, T.; Percheron-Guégan, A. *Chem. Commun.* **2003**, 2976. (c) Rowsell, J. L.; Millward, A. R.; Park, K. S.; Yaghi, O. M. *J. Am. Chem. Soc.* **2004**, *126*, 5666. (d) Lee, E. Y.; Suh, M. P. *Angew. Chem., Int. Ed.* **2004**, *43*, 2798. (e) Sun, D.; Ma, S.; Ke, Y.; Collins, D. J.; Zhou, H.-C. *J. Am. Chem. Soc.* **2006**, *128*, 3896. (f) Wong-Foy, A. G.; Matzger, A. J.; Yaghi, O. M. *J. Am. Chem. Soc.* **2006**, *128*, 3494. (g) Lin, X.; Jia, J.; Zhao, X.; Thomas, K. M.; Blake, A. J.; Walker, G. S.; Champness, N. R.; Hubberstey, P.; Schröder, M. *Angew. Chem., Int. Ed.* **2006**, *45*, 7358. (h) Latroche, M.; Surlblé, S.; Serre, C.; Mellot-Drazniéks, C.; Llewellyn, P. L.; Lee, J.-H.; Chang, J.-S.; Jhung, S. H.; Férey, G. *Angew. Chem., Int. Ed.* **2006**, *45*, 8227. (i) Xiao, B.; Wheatley, P. S.; Zhao, X.; Fletcher, A. J.; Fox, S.; Rossi, A. G.; Megson, I. L.; Bordiga, S.; Regli, L.; Thomas, K. M.; Morris, R. E. *J. Am. Chem. Soc.* **2007**, *129*, 1203. (j) Kaye, S. S.; Dailly, A.; Yaghi, O. M.; Long, J. R. *J. Am. Chem. Soc.* **2007**, *129*, 14176. (k) Sumida, K.; Hill, M. R.; Horike, S.; Dailly, A.; Long, J. R. *J. Am. Chem. Soc.* **2009**, *131*, 15120. (l) Murray, L. J.; Dincă, M.; Long, J. R. *Chem. Soc. Rev.* **2009**, *38*, 1294 and references therein.

(4) Bhatia, S. K.; Myers, A. L. *Langmuir* **2006**, *22*, 1688.

(5) (a) Garrone, E.; Bonelli, B.; Otero Areán, C. *Chem. Phys. Lett.* **2008**, *456*, 68. (b) Otero Areán, C.; Chavan, S.; Cabello, C. P.; Garrone, E.; Palomino, G. T. *ChemPhysChem* **2010**, *11*, 3237.

(6) (a) Dietzel, P. D. C.; Morita, Y.; Blom, R.; Fjellvag, H. *Angew. Chem., Int. Ed.* **2005**, *44*, 6354. (b) Dincă, M.; Long, J. R. *J. Am. Chem. Soc.* **2005**, *127*, 9376. (c) Rosi, N. L.; Kim, J.; Eddaoudi, M.; Chen, B.; O’Keeffe, M.; Yaghi, O. M. *J. Am. Chem. Soc.* **2005**, *127*, 1504. (d) Vimont, A.; Goupil, J.-M.; Lavalley, J.-C.; Daturi, M.; Surlblé, S.; Serre, C.; Millange, F.; Férey, G.; Audebrand, N. *J. Am. Chem. Soc.* **2006**, *128*, 3218. (e) Moon, H. R.; Kobayashi, N.; Suh, M. P. *Inorg. Chem.* **2006**, *45*, 8672. (f) Dincă, M.; Dailly, A.; Liu, Y.; Brown, C. M.; Neumann, D. A.; Long, J. R. *J. Am. Chem. Soc.* **2006**, *128*, 16876. (g) Dietzel, P. D. C.; Panella, B.; Hirscher, M.; Blom, R.; Fjellvag, H. *Chem. Commun.* **2006**, 959. (h) Dincă, M.; Han, W. S.; Liu, Y.; Dailly, A.; Brown, C. M.; Long, J. R. *Angew. Chem., Int. Ed.* **2007**, *46*, 1419. (i) Dincă, M.; Long, J. R. *Angew. Chem., Int. Ed.* **2008**, *47*, 6766. (j) Caskey, S. R.; Wong-Foy, A. G.; Matzger, A. J. *J. Am. Chem. Soc.* **2008**, *130*, 10870. (k) Dietzel, P. D. C.; Blom, R.; Fjellvag, H. *Eur. J. Inorg. Chem.* **2008**, 3624. (l) Liu, Y.; Kabbour, H.; Brown, C. M.; Neumann, D. A.; Ahn, C. C. *Langmuir* **2008**, *24*, 4772. (m) Dietzel, P. D. C.; Johnsen, R. E.; Fjellvag, H.; Bordiga, S.; Groppo, E.; Chavan, S.; Blom, R. *Chem. Commun.* **2008**, 5125. (n) Zhou, W.; Wu, H.; Yildirim, T. *J. Am. Chem. Soc.* **2008**, *130*, 15268. (o) Dietzel, P. D. C.; Besikiotis, V.; Blom, R. *J. Mater. Chem.* **2009**, *19*, 7362. (p) Sumida, K.; Horike, S.; Kaye, S. S.; Herm, Z. R.; Queen, W. L.; Brown, C. M.; Grandjean, F.; Long, G. J.; Dailly, A.; Long, J. R. *Chem. Sci.* **2010**, *1*, 184.

(7) Belof, J. L.; Stern, A. C.; Eddaoudi, M.; Space, B. *J. Am. Chem. Soc.* **2007**, *129*, 15202.

(8) Cheon, Y. E.; Suh, M. P. *Chem. Commun.* **2009**, 2296.

(9) Vitillo, J. G.; Regli, L.; Chavan, S.; Ricchiardi, G.; Spoto, G.; Dietzel, P. D. C.; Bordiga, S.; Zecchina, A. *J. Am. Chem. Soc.* **2008**, *130*, 8386.

(10) (a) Frost, H.; Düren, T.; Snurr, R. Q. *J. Phys. Chem. B* **2006**, *110*, 9565. (b) Han, S. S.; Deng, W.-Q.; Goddard, W. A. *Angew. Chem., Int. Ed.* **2007**, *46*, 6289. (c) Han, S. S.; Goddard, W. A. *J. Am. Chem. Soc.* **2007**, *129*, 8422. (d) Thornton, A. W.; Nairn, K. M.; Hill, J. M.; Hill, A. J.; Hill, M. R. *J. Am. Chem. Soc.* **2009**, *131*, 10662. (e) Han, S. S.; Furukawa, H.; Yaghi, O. M.; Goddard, W. A. *J. Am. Chem. Soc.* **2009**, *131*, 11580. (f) Düren, T.; Bae, Y.-S.; Snurr, R. Q. *Chem. Soc. Rev.* **2009**, *38*, 1237 and references therein.

(11) Murray, L. J.; Dincă, M.; Yano, J.; Chavan, S.; Bordiga, S.; Brown, C. M.; Long, J. R. *J. Am. Chem. Soc.* **2010**, *132*, 7856.

(12) (a) Chui, S. S.-Y.; Lo, S. M.-F.; Charmant, J. P. H.; Orpen, A. G.; Williams, I. D. *Science* **1999**, *283*, 1148. (b) Vishnyakov, A.; Ravikovitch, P. I.; Neimark, A. V.; Bülow, M.; Wang, Q. M. *Nano Lett.* **2003**, *3*, 713. (c) Bordiga, S.; Regli, L.; Bonino, F.; Groppo, E.; Lamberti, C.; Xiao, B.; Wheatley, P. S.; Morris, R. E.; Zecchina, A. *Phys. Chem. Chem. Phys.* **2007**, *9*, 2676.

(13) Despite the ubiquitous nature of molecular paddlewheel chemistry, reports of metal–organic frameworks exhibiting the  $M_3(\text{BTC})_2$  ( $M = \text{Cr}, \text{Cu}$ ) structure type have been relatively limited.  $\text{Mo}_3(\text{BTC})_2$ : Kramer, M.; Schwarz, U.; Kaskel, S. *J. Mater. Chem.* **2006**, *16*, 2245.  $[\text{Fe}_2(\text{H}_2\text{O})_2(\text{BTC})_{4/3}]\text{Cl}\cdot 4.5(\text{DMF})$ : Xie, L.; Liu, S.; Gao, C.; Cao, R.; Cao, J.; Sun, C.; Su, Z. *Inorg. Chem.* **2007**, *46*, 7782.

(14) Certain commercial suppliers are identified in this paper to foster understanding. Such identification does not imply recommendation or endorsement by the National Institute of Standards and Technology, nor does it imply that the materials or equipment identified are necessarily the best available for the purpose.

(15) Toby, B. H. *J. Appl. Crystallogr.* **2001**, *34*, 210.

(16) Larson, A. C.; Von Dreele, R. B. *General Structure Analysis System (GSAS)*, Los Alamos National Laboratory Report LAUR 86-748, 2000.

(17) Brown, C. M.; Liu, Y.; Yildirim, T.; Peterson, V. K.; Kepert, C. J. *Nanotechnology* **2009**, *20*, 204025.

(18) Udovic, T. J.; Brown, C. M.; Leao, J. B.; Brand, P. C.; Jiggetts, R. D.; Zeitoun, R.; Pierce, T. A.; Peral, I.; Copley, J. R. D.; Huang, Q.; Neumann, D. A.; Fields, R. J. *Nucl. Instrum. Methods Phys. Res., Sect. A* **2008**, *588*, 406.

(19) Azuah, R. T.; Kneller, L. R.; Qiu, Y.; Tregenna-Piggott, P. L. W.; Brown, C. M.; Copley, J. R. D.; Dimeo, R. M. *J. Res. Natl. Inst. Stand. Technol.* **2009**, *114*, 241.

(20) FitzGerald, S. A.; Churchill, H. O. H.; Korngut, P. M.; Simmons, C. B.; Strangas, Y. E. *Rev. Sci. Instrum.* **2006**, *77*, 093110.

(21) Rowsell, J. L. C.; Yaghi, O. M. *J. Am. Chem. Soc.* **2006**, *128*, 1304.

(22) Peterson, V. K.; Liu, Y.; Brown, C. M.; Kepert, C. J. *J. Am. Chem. Soc.* **2006**, *128*, 15578.

(23) The shortest  $M^{2+}-D_2$  distance directly observed to date within a metal–organic framework via neutron diffraction is 2.15(4) Å observed within  $\text{Fe}_3[(\text{Fe}_4\text{Cl})_3(\text{BTT})_8]_2$  ( $\text{Fe}-\text{BTT}$ ,  $\text{BTT}^{3-} = 1,3,5$ -benzenetrisulfonate), which features unsaturated  $\text{Fe}^{2+}$  coordination sites; see ref 6p.

(24) Ramirez-Cuesta, A. J.; Mitchell, P. C. H.; Ross, D. K.; Georgiev, P. A.; Anderson, P. A.; Langmi, H. W.; Book, D. *J. Mater. Chem.* **2007**, *17*, 2533.

(25) Note that the correlation between the neutron scattering data and infrared data is not definitive owing to the difference in the conditions (temperature and loading level) employed for the two types of experiments. While the analysis presented here allows the greatest degree of consistency and agreement between the two types of data, we envisage a number of alternative scenarios for peak assignment (particularly for site I and II), if the infrared data alone is considered.

## NOTE ADDED AFTER ASAP PUBLICATION

This article was published ASAP on March 25, 2011. A text correction has been made in the last paragraph before the Conclusions and another in ref 23. The correct version was published on April 1, 2011.